

The Role of Photodissociation Regions in Massive Star Formation

Joseph L. Hora, Lori E. Allen, S. Thomas Megeath, Lynne K. Deusch, Giovanni G. Fazio
Harvard-Smithsonian Center for Astrophysics



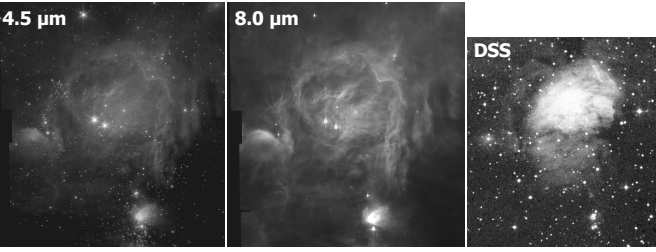
Abstract

The evolution of high mass star formation regions is affected by the creation and evolution of photodissociation regions (PDRs), which are not present in the case of low mass star formation since stars in the latter do not emit the necessary UV. In star forming regions like AFGL 4029, NGC 7538, and S252, high mass YSOs representing a second generation of star formation are often found embedded in PDRs. Because of their proximity to HII regions, these clusters are also good laboratories for the study of "sequential" or "triggered" star formation, in which an expanding HII region compresses the molecular gas and induces star formation along the ionization front at the molecular cloud/HII region interface. In order to understand how the chemistry, composition, and structure of PDRs fit into the overall puzzle of high mass star formation, we have undertaken a program of high sensitivity IRAC imaging of the infrared emission from these regions. Three of IRAC's four bands include wavelengths of emission from PAHs, which are excellent diagnostics for probing the conditions in PDRs through spectral and spatial variations. We present results from the IRAC images of the first objects in this survey.

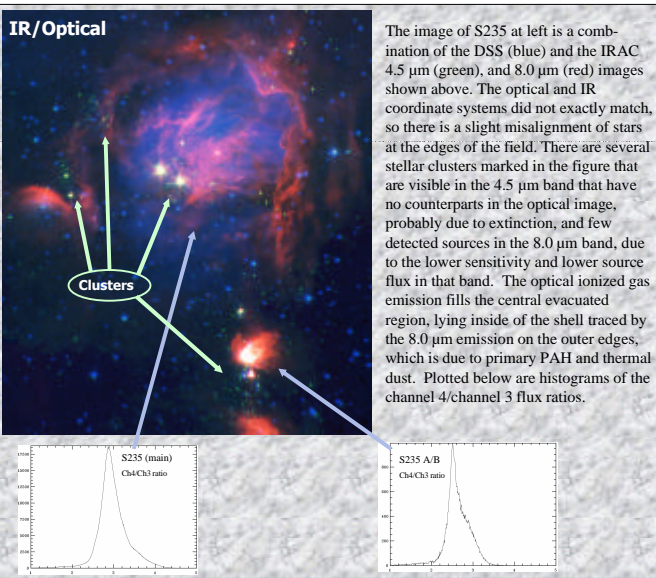
PDR program

We have a survey in process of several regions of high-mass star formation using IRAC to assess their content and structure. The table at right shows the star forming regions in our sample. These regions were originally selected for the IRAC observations on the basis of the following criteria: 1) they have extended PDRs suitable for modeling, as identified in MSX or other pre-existing data sets; 2) emit strongly at mid-IR wavelengths; 3) exhibit masers, which are signposts of massive star formation; 4) contain UCHII regions identified in radio surveys; and 5) are at distances of <4 kpc, to allow us to resolve structure greater than 0.05 pc with IRAC imaging.

Target	RA	Dec
NGC 7538	23h13m42.00s	+61d30m10.0s
S88	19h46m43.00s	+25d12m14.0s
S252	06h09m04.70s	+20d35m09.0s
AFGL 437	03h07m53.00s	+58d35m03.0s
S235	05h41m00.00s	+35d48m04.0s
AFGL 4029	03h02m00.00s	+60d33m49.0s
S255	06h12m46.00s	+18d00m38.0s
S87	19h46m17.00s	+24d39m03.0s
S76	18h56m07.00s	+07d56m03.0s



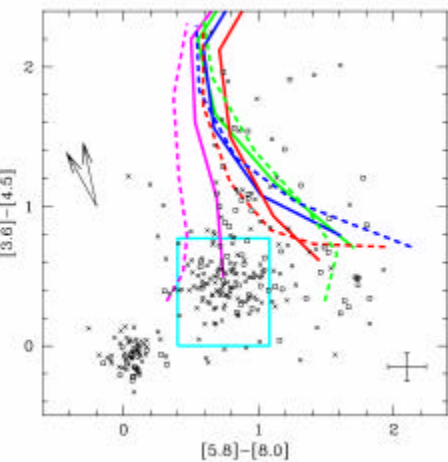
Shown above are images from the IRAC 3.6 and 8.0 μm channels, and the Digital Sky Survey (DSS) image of the same field, displayed with a logarithmic stretch. These images are combined in the image below. The 8.0 μm band samples the 7.7 μm PAH feature, the 4.5 μm band contains no PAH features.



The image above is a four-color image of S235, with the IRAC 3.6, 4.5, 5.8, and 8.0 μm bands mapped from blue to red. This image is approximately 18 x 20 arcmin in size, or 9.4 x 10.5 pc. The main S235 source is the large cloud in the upper part of the image, the two smaller bright clouds below are S235A/B, and S235C. Emission in the 3.6, 5.8, and 8.0 μm bands is dominated by the broad PAH features at 3.3, 6.2, and 7.7 μm (Krassner et al. 1982). The ratio of the 5.8 to 8.0 μm band fluxes over the entire extended emission region of the main S235 source is remarkably constant, having a ratio of 3.0 ± 0.2 . The band ratio over S235A/B is also flat over the source, but at a different value: 2.5 ± 0.1 (see histograms in the figure at left). This points to different excitation conditions of the PAH emission, or differences in the temperature of the dust, possibly due to the different UV fields in the two regions.

IRAC Colors of sources

Measured IRAC colors for S235 (x's) and S255 (?), and model colors from Allen et al. (2004). Representative error bars, including average photometric uncertainties and an estimated 10% uncertainty in the absolute flux calibration, are shown. The light blue square delineates the approximate domain of Class II (disk) sources. Disk models have stars with $T_{\text{eff}}=4000\text{K}$, $t=1\text{ Myr}$ and span accretion rates of $\log \dot{M} = -9$ to $-6 M_{\odot}/\text{yr}$. Two inclinations (30° and 60°) and two disk radii ($R_d = 100$ and 300 AU) were considered. Colored lines show Class I (envelope) sources. Envelope models are shown for a range of central source luminosities, color coded as magenta, green, blue, red = 0.1, 1, 10 and $100 L_{\odot}$ respectively. Envelope densities are shown for $\log \rho_1 = -14, -13.5, -13.35, -13, -12.75$, and -12.5 g/cm^3 , increasing from bottom to top. Models are plotted for two values of the centrifugal radius $R_c = 50\text{ AU}$ (solid line), and 300 AU (dashed line), and one inclination (60°). Extinction vectors are shown for $A_v = 30$ using the two extremes of the six vectors calculated by Megeath et al. (2004). The vector on the left is for a flat spectrum source and Draine & Lee (1984) extinction law, while the vector to the right is for a Vega spectrum and the extinction law of Mathis (1990).



References:

Allen, L. E., Calvet, N., D'Alessio, P., Merin, B., Hartmann, L., Megeath, S. T., Gutermuth, R. A., Muzerolle, J., Pipher, J. L., Myers, P. C., & Fazio, G. G. 2004, *ApJS*, 154, in press
 Draine, B. T. & Lee, H. M. 1984, *ApJ*, 285, 89
 Krassner, J., Pipher, J. L., Sharpless, S., Herter, T., 1982, *A&A*, 109, 223
 Mathis, J. S. 1990, *ARA&A*, 28, 37
 Megeath, S. T., L.E. Allen, R.A. Gutermuth, J.L. Pipher, P.C. Myers, N. Calvet, L. Hartmann, J. Muzerolle, & G.G. Fazio 2004, *ApJS*, 154, in press

Acknowledgments:

This work is based on observations made with the Spitzer Space Telescope, which is operated by the Jet Propulsion Laboratory, California Institute of Technology under NASA contract 1407. Support for this work was provided by NASA.

Lynne Deusch, the original P.I. of this project, passed away on April 2 after a long illness. She will be deeply missed by her friends and colleagues on the IRAC team.